Loss of myeloid lipoprotein lipase exacerbates adipose tissue fibrosis with collagen VI deposition and hyperlipidemia in leptin-deficient obese mice

Received for publication, January 21, 2022, and in revised form, July 19, 2022 Published, Papers in Press, August 1, 2022,
https://doi.org/10.1016/j.jbc.2022.102322

Manabu Takahashi[1,*], Daisuke Yamamuro[1], Tetsuji Wakabayashi[1], Akihito Takei[1], Shoko Takei[1], Shuichi Nagashima[1], Hiroaki Okazaki[1], Ken Ebihara[1], Hiroaki Yagyu[1], Yuki Takayanagi[2], Tatsushi Onaka[2], Ira J. Goldberg[3], and Shun Ishibashi[1,*]

From the [1]Division of Endocrinology and Metabolism, Department of Internal Medicine, School of Medicine, Jichi Medical University, Tochigi, Japan; [2]Division of Brain and Neurophysiology, Department of Physiology, School of Medicine, Jichi Medical University, Tochigi, Japan; [3]NYU-Langone Medical Center, New York, New York, USA

Edited by Qi-Qun Tang

During obesity, tissue macrophages increase in number and become proinflammatory, thereby contributing to metabolic dysfunction. Lipoprotein lipase (LPL), which hydrolyzes triglyceride in lipoproteins, is secreted by macrophages. However, the role of macrophage-derived LPL in adipose tissue remodeling and lipoprotein metabolism is largely unknown. To clarify these issues, we crossed leptin-deficient *Lep*$^{ob/ob}$ mice with mice lacking the *Lpl* gene in myeloid cells (*Lpl*$^{m-/m-}$) to generate *Lpl*$^{m-/m-}$;*Lep*$^{ob/ob}$ mice. We found the weight of perigonadal white adipose tissue (WAT) was increased in *Lpl*$^{m-/m-}$;*Lep*$^{ob/ob}$ mice compared with *Lep*$^{ob/ob}$ mice due to substantial accumulation of both adipose tissue macrophages and collagen that surrounded necrotic adipocytes. In the fibrotic epididymal WAT of *Lpl*$^{m-/m-}$;*Lep*$^{ob/ob}$ mice, we observed an increase in collagen VI and high mobility group box 1, while α-smooth muscle cell actin, a marker of myofibroblasts, was almost undetectable, suggesting that the adipocytes were the major source of the collagens. Furthermore, the adipose tissue macrophages from *Lpl* $^{m-/m-}$;*Lep*$^{ob/ob}$ mice showed increased expression of genes related to fibrosis and inflammation. In addition, we determined *Lpl* $^{m-/m-}$;*Lep*$^{ob/ob}$ mice were more hypertriglyceridemic than *Lep*$^{ob/ob}$ mice. *Lpl*$^{m-/m-}$;*Lep*$^{ob/ob}$ mice also showed slower weight gain than *Lep*$^{ob/ob}$ mice, which was primarily due to reduced food intake. In conclusion, we discovered that the loss of myeloid *Lpl* led to extensive fibrosis of perigonadal WAT and hypertriglyceridemia. In addition to illustrating an important role of macrophage LPL in regulation of circulating triglyceride levels, these data show that macrophage LPL protects against fibrosis in obese adipose tissues.

Obesity, which is pandemic in most parts of the world, is characterized by chronic and low-grade inflammation (1). Within white adipose tissue (WAT) from obese mice and humans, crown-like structures are created by adipose tissue macrophages (ATMs) (2), which scavenge lipid droplets released by dying adipocytes. ATMs, which produce proinflammatory cytokines, might also contribute to insulin resistance (3). Obesity is also accompanied by excessive deposition of extracellular matrix within adipose tissues (4). As adipose tissue expands, local hypoxia induces the expression of hypoxia-inducible factor 1α in adipocytes, which conceivably mediates the fibrotic response in obesity (5). ATMs are also involved in the development of adipose tissue fibrosis (6). Obese mice develop hepatic steatosis with increased number of recruited hepatic macrophages (7).

Lipoprotein lipase (LPL) hydrolyzes triglycerides (TGs) in chylomicrons and very-low-density lipoprotein (VLDL), thereby liberating free fatty acids (FFAs) (8). This lipolytic reaction takes place at the luminal side of capillary endothelial cells, on which LPL is tethered to proteoglycans and glycosylphosphatidylinositol-anchored high-density lipoprotein-binding protein 1 after translocation from its sites of synthesis. LPL is synthesized by various cells including adipocytes, cardiomyocytes, skeletal muscle cells, and macrophages. LPL activity requires correct folding, which is mediated by lipase maturation factor 1. Macrophages also synthesize LPL, where its actions might be exclusive of regulation of circulating TG levels (9).

In vitro studies showed that LPL secreted from macrophages stimulates foam cell formation by converting VLDL to lipoproteins with high affinity for lipoprotein receptors (10), increasing uptake of lipoproteins by acting as a receptor ligand, or by increasing the approximation of lipoproteins to the cell surface (11). Not surprisingly, macrophage LPL associates with greater atherosclerosis. Indeed, several laboratories including ours showed that mice lacking *Lpl* in bone marrow or due to a macrophage specific knockout had reduced atherosclerosis (12–14). Consistently, mice overexpressing *Lpl* in macrophages (15) or with LPL activity increased due to a deficiency of its inhibitor angiopoietin-like protein 4 (16) showed increased atherosclerosis. Moreover, the amount of LPL activity within an artery directly correlates with the extent of

* For correspondence: Shun Ishibashi, ishibash@jichi.ac.jp; Manabu Takahashi, m-taka@jichi.ac.jp.

atherosclerosis (17), and this LPL is primarily expressed in macrophages (18, 19).

Because ATMs comprise as much as 50% of the cells in adipose tissue in severe obesity (20), we hypothesized that myeloid cell *Lpl* deficiency would decrease lipid accumulation in adipocytes by limiting the supply of lipoprotein-derived FFA. It is also possible that myeloid cell *Lpl* deficiency would ameliorate adipose tissue inflammation, because FFA generated during lipolysis might be proinflammatory (21). Together with the increased number of ATMs, the increased number of recruited hepatic macrophages in obese mice can substantially affect plasma lipoprotein metabolism via changing tissue LPL activity.

However, our previous study using *Apoe*$^{-/-}$ and *Apoe*-deficient mice lacking *Lpl* in myeloid cells (*Lpl*$^{m-/m-}$;*Apoe*$^{-/-}$) fed a Western-type diet for 12 weeks revealed no differences in body weight, weights of gonadal fat pad, or expression of genes specific for macrophages or inflammation in WAT (14). Similarly, a combined adipose and macrophage knockout had only minor effects on white adipose development and histology (22). This caused us to question whether the obesogenic effects of the Western-type diet were insufficient to see alterations in adipose tissue, especially in the setting of apoE deficiency (23).

To circumvent the limitation of the use of Western-type diet feeding, we used leptin-deficient *Lep*$^{ob/ob}$ mice in the present study. Because *Lep*$^{ob/ob}$ mice are more obesogenic than the Western-type diet, the use of *Lep*$^{ob/ob}$ mice can allow us to detect the effects of myeloid cell *Lpl* deficiency on obesity-related phenotypes. We found that *Lep*$^{ob/ob}$ mice lacking *Lpl* in myeloid cells (*Lpl*$^{m-/m-}$;*Lep*$^{ob/ob}$) fed a regular laboratory diet developed more extensive fibrosis in epididymal WAT (eWAT) and hypertriglyceridemia than *Lep*$^{ob/ob}$ mice, while they had lower body weight. The ATMs of *Lpl*$^{m-/m-}$;*Lep*$^{ob/ob}$ mice showed increased expression of fibrogenic genes compared with those of *Lep*$^{ob/ob}$ mice. Thus, myeloid cell–derived *Lpl* has a critical role in the regulation of adipose tissue fibrosis during the development of obesity.

Results

Loss of myeloid Lpl *exacerbated fibrosis in WAT in* Lep$^{ob/ob}$ *background*

By gross inspection, eWAT from *Lpl*$^{m-/m-}$;*Lep*$^{ob/ob}$ mice was more brownish compared with that from *Lep*$^{ob/ob}$ mice at the age of 24 weeks (Fig. 1*A*). Female perigonadal fat from *Lpl*$^{m-/m-}$;*Lep*$^{ob/ob}$ mice also showed the same appearance (data not shown). Adipocytes were significantly smaller in *Lpl*$^{m-/m-}$;*Lep*$^{ob/ob}$ mice than in *Lep*$^{ob/ob}$ mice by 27% at the age of 24 weeks (Fig. 1, *B* and *C*), while adipocyte number per area did not differ between *Lep*$^{ob/ob}$ and *Lpl*$^{m-/m-}$;*Lep*$^{ob/ob}$ mice (Fig. 1*D*). Masson's trichrome and Sirius red staining revealed that the fibrotic areas were increased in *Lpl*$^{m-/m-}$;*Lep*$^{ob/ob}$ mice compared with *Lep*$^{ob/ob}$ mice by 3.7- and 7.3-fold, respectively (Fig. 1, *E–H*). Consistent with these results, eWAT collagen content was increased in *Lpl*$^{m-/m-}$;*Lep*$^{ob/ob}$ mice compared with *Lep*$^{ob/ob}$ mice by 1.8-fold (Fig. 1*I*). eWAT TG content per gram of tissue in *Lpl*$^{m-/m-}$;*Lep*$^{ob/ob}$ mice was reduced compared with *Lep*$^{ob/ob}$ by 36% (Fig. 1, *J*). On the other hand, eWAT TG content per whole tissue was not different between the two groups (Fig. 1, *K*). The number of necrotic perilipin-negative adipocytes surrounded by Mac-2-positive macrophages was increased in *Lpl*$^{m-/m-}$;*Lep*$^{ob/ob}$ mice compared with *Lep*$^{ob/ob}$ mice by 4.7-fold (Fig. 2).

Similarly, perirenal fat from *Lpl*$^{m-/m-}$;*Lep*$^{ob/ob}$ mice was more brownish compared with that from *Lep*$^{ob/ob}$ mice (Fig. 3*A*). Moderate but significant interstitial changes were also observed in the perirenal fat from *Lpl*$^{m-/m-}$;*Lep*$^{ob/ob}$ mice (Fig. 3*B*). Furthermore, inguinal subcutaneous fat from *Lpl*$^{m-/m-}$;*Lep*$^{ob/ob}$ mice was a little more brownish compared with that from *Lep*$^{ob/ob}$ mice (Fig. 3*D*). Mild interstitial changes were also observed in the subcutaneous fat from *Lpl*$^{m-/m-}$;*Lep*$^{ob/ob}$ mice (Fig. 3*E*). Unlike eWAT, perirenal and subcutaneous adipocyte sizes were not different between *Lep*$^{ob/ob}$ and *Lpl*$^{m-/m-}$;*Lep*$^{ob/ob}$ mice (Fig. 3, *C* and *F*).

The expression of fibrosis-related genes and collagen VI (Col6) is increased in WAT from Lpl$^{m-/m-}$;Lep$^{ob/ob}$ *mice*

To determine whether the brownish appearance of eWAT from *Lpl*$^{m-/m-}$;*Lep*$^{ob/ob}$ mice reflected browning (enrichment of beige adipocytes) or inflammatory and fibrotic changes in the eWAT from *Lpl*$^{m-/m-}$;*Lep*$^{ob/ob}$ mice, we measured mRNA levels of *uncoupling protein 1* (*Ucp1*), macrophage marker genes, and genes involved in inflammation and fibrosis in the eWAT at the age of 24 weeks. The expression of *Ucp1* was not increased in *Lpl*$^{m-/m-}$;*Lep*$^{ob/ob}$ compared with *Lep*$^{ob/ob}$ mice (Fig. 4*A*), indicating that browning, an increase in the number of beige adipocytes, did not cause brownish coloring of the eWAT of *Lpl*$^{m-/m-}$;*Lep*$^{ob/ob}$ mice. We did note an increase in expression levels of macrophage markers in these mice. *Cd68* and *F4/80* were expressed at much higher levels with the *ob/ob* background (Fig. 4*B*). *Cd68* and *Cd11b* were 81% and 4.4-fold higher in *Lpl*$^{m-/m-}$;*Lep*$^{ob/ob}$ than in *Lep*$^{ob/ob}$ mice, respectively, although the absence of *Lpl* did not markedly affect the expression levels of *F4/80* or *Cd11b* on the wildtype background (Fig. 4*B*).

We next checked the expression levels of proinflammatory M1 macrophage markers (*Cd11c*, *Tnfa*, *monocyte chemotactic protein-1* (*Mcp1*), *Il6*, and *Nos2*) (Fig. 4*C*). *Cd11c* and *Tnfa* were expressed at much higher levels with the *ob/ob* background. The mRNA expression of *Cd11c* and *Il6* were 3.2-fold and 5.8-fold higher in *Lpl*$^{m-/m-}$;*Lep*$^{ob/ob}$ than in *Lep*$^{ob/ob}$ mice, respectively, while there were no significant differences in the mRNA expression of *Tnfa, Mcp1, and Nos2* between the two groups.

With regard to the expression levels of anti-inflammatory M2 macrophage markers (Fig. 4*D*), *Il10* was expressed at higher levels, while Fizz1 (also known as *resistin like alpha* [*Retnla*]) was expressed at lower levels compared with *ob/ob* background. *Lpl*$^{m-/m-}$;*Lep*$^{ob/ob}$ mice had significantly higher mRNA levels of *Cd206* than *Lep*$^{ob/ob}$ mice, while *Lpl*$^{m-/m-}$;*Lep*$^{ob/ob}$ mice had significantly lower levels of *Fizz1* than *Lep*$^{ob/ob}$ mice. There was no difference in the expression of either *Il10* or *Arg1* between *Lep*$^{ob/ob}$ and *Lpl*$^{m-/m-}$;*Lep*$^{ob/ob}$ mice.

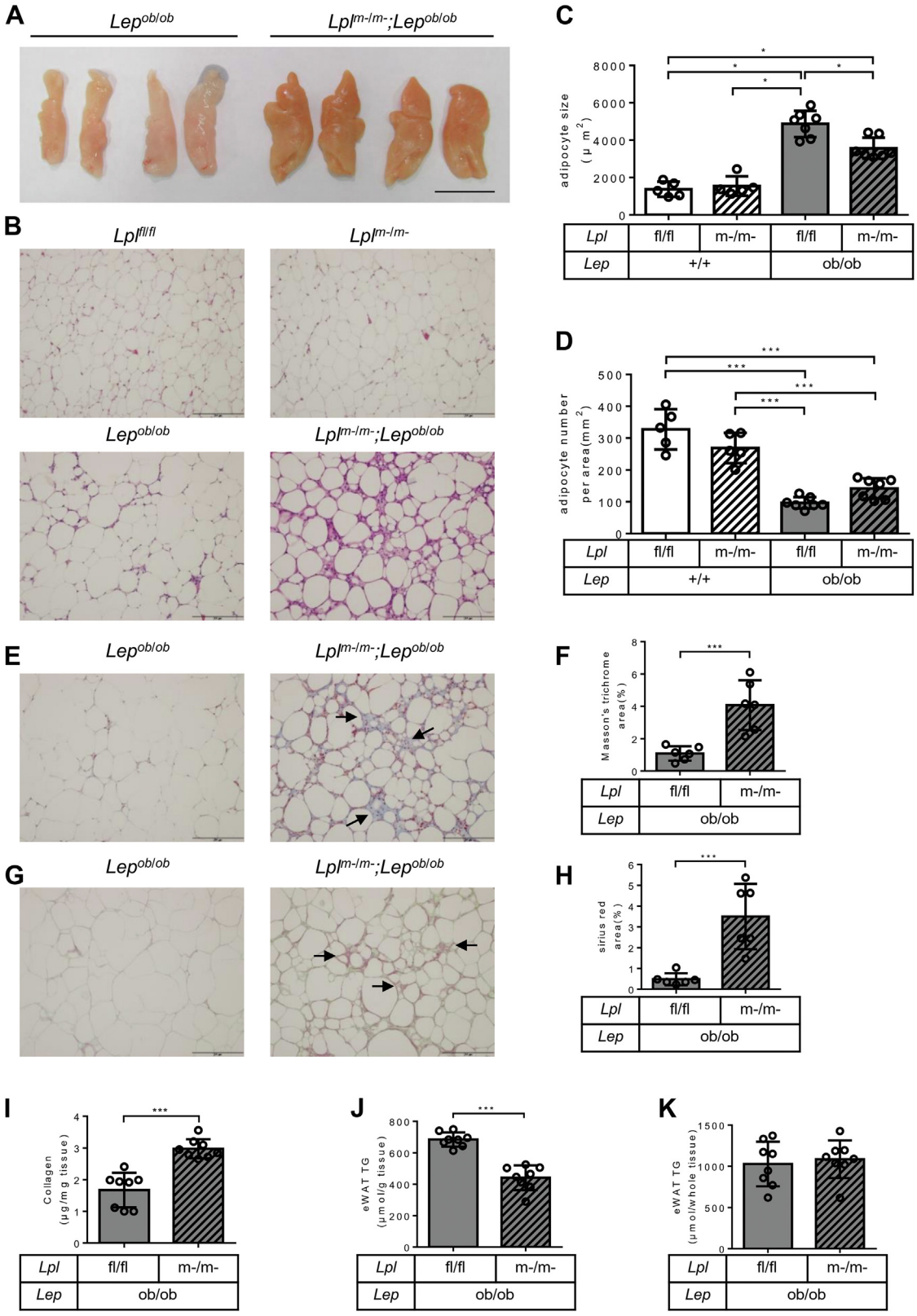

Figure 1. Loss of myeloid *Lpl* augments adipose tissue fibrosis in *Lep*$^{ob/ob}$ mice. (*A*) gross appearance of eWAT at the age of 24 weeks. Two mice fat pads are shown in each genotype. The scale bar represents 2 cm. (*B*) histology of eWAT stained with H&E. (*C, D*) the average adipocyte size and number of adipocytes per area in eWAT were quantified (n=5–7). (*E, F*) Masson's trichrome staining in eWAT and quantification of Masson's trichrome–positive areas (indicated by an arrow) (n = 6). (*G, H*) Sirius red staining in eWAT and quantification of Sirius red–positive areas (indicated by an arrow) (n = 6). (*I*) collagen content in eWAT. (*J*) eWAT TG content per gram of tissue (n = 8). (*K*) eWAT TG content per whole tissue was calculated by multiplying the whole tissue weight (n = 8). The scale bar represents 200 μm (*B, E, G*). Values are expressed as means ± SD. *$p < 0.05$, ***$p < 0.001$. eWAT, epididymal white adipose tissue; TG, triglyceride.

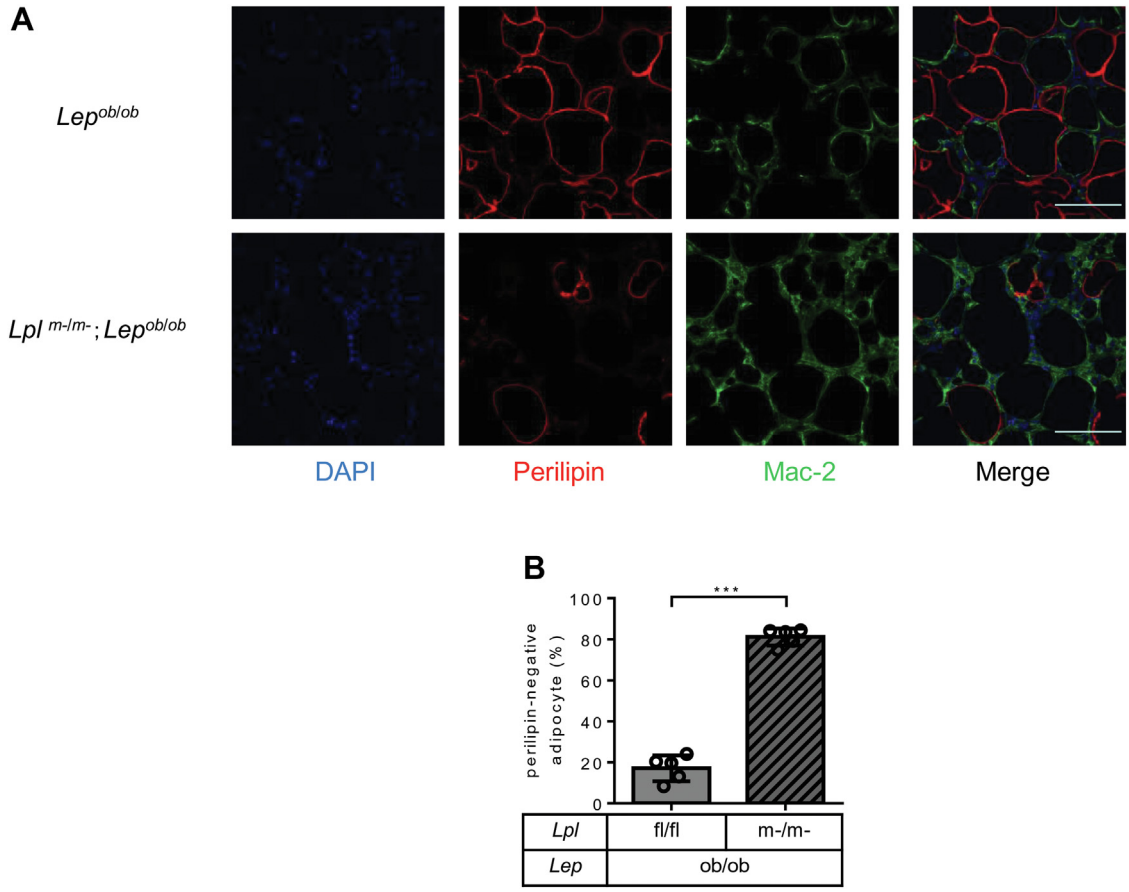

Figure 2. Immunofluorescent staining for necrotic adipocytes surrounded with macrophages. (*A*) representative immunofluorescent staining for DAPI (blue), perilipin (red), and Mac-2 (green) in eWAT. The scale bar represents 100 μm. (*B*) quantification of perilipin-negative adipocytes (n = 5). Values are expressed as means ± SD. ***$p < 0.001$

Finally, we checked the expression levels of the genes related to fibrosis, *Hif1a*, *Tgfb1*, *tissue inhibitor of metalloproteinase 1 (Timp1)*, *Col1a1*, *Col3a1*, *Col6a3,* and *Acta2* (Fig. 4*E*). *Tgfb1*, *Timp1*, *Col1a1*, *Col3a1,* and *Col6a3* were significantly higher in $Lpl^{m-/m-}$;$Lep^{ob/ob}$ than in $Lep^{ob/ob}$ mice by 36%, 186%, 104%, 58%, and 74%, respectively. The expression of *Acta2* (also known as α-smooth muscle actin, a marker of fibrogenic myofibroblasts (24), was significantly decreased in $Lpl^{m-/m-}$;$Lep^{ob/ob}$ mice.

To confirm the findings in the mRNA expression at the protein level, we performed immunoblot analyses of Acta2, Timp1, Col1, Col3, and Col6 in the eWAT (Fig. 5*A*). Consistent with the gene expression, Acta2 protein was markedly decreased in $Lpl^{m-/m-}$;$Lep^{ob/ob}$ mice. Timp1 protein was not significantly different between four groups of mice. Among the three types of collagen, the changes in Col6 were most striking; $Lpl^{m-/m-}$;$Lep^{ob/ob}$ mice had a 5.5-fold higher content of Col6 in eWAT than $Lpl^{fl/fl}$ mice (Fig. 5*B*). Similar to the expression pattern of Col6, $Lpl^{m-/m-}$;$Lep^{ob/ob}$ mice had a 2.9-fold higher content of high mobility group box 1 (HMGB1) protein, a nuclear nonhistone DNA-binding protein that is implicated in inflammation and efferocytosis (25), in eWAT than $Lep^{ob/ob}$ mice (Fig. 5, *A* and *B*). Although the protein contents of the eWAT of $Lpl^{m-/m-}$;$Lep^{ob/ob}$ mice were 2- to 3-fold higher than those of $Lpl^{fl/fl}$, $Lpl^{m-/m-}$, or $Lep^{ob/ob}$ mice ($Lpl^{fl/fl}$, 11.0 ± 2.3 mg/g; $Lpl^{m-/m-}$, 13.1± 1.7 mg/g; $Lep^{ob/ob}$, 11.4 ± 1.9 mg/g; $Lpl^{m-/m-}$;$Lep^{ob/ob}$, 30.8 ± 4.2 mg/g wet tissue, n = 6), we loaded the same amounts of proteins (30 μg) to each lane of the gels. Therefore, the increases in the protein levels of collagens, Timp1, and HMGB1 should be much higher than the above values when expressed per wet tissue weight.

We also measured mRNA levels of the genes in subcutaneous fat (Fig. 6), which was less fibrotic than eWAT in $Lpl^{m-/m-}$;$Lep^{ob/ob}$ mice (Fig. 3, *D* and *E*). The mRNA expression patterns were essentially similar to those in eWAT, except that the induction of the expression of *Cd206*, *Col1a1*, *Col3a1,* and *Col6a3* in $Lpl^{m-/m-}$;$Lep^{ob/ob}$ mice compared with in $Lep^{ob/ob}$ mice was not observed, corroborating the morphological findings that there was no significant difference in the extent of fibrosis in subcutaneous fat between $Lep^{ob/ob}$ and $Lpl^{m-/m-}$;$Lep^{ob/ob}$ mice (Fig. 3*E*).

The expression of fibrosis-related genes is increased in ATMs from $Lpl^{m-/m-}$;$Lep^{ob/ob}$ *mice*

To determine whether the changes in fibrotic genes were due to macrophages or other cells within the eWAT, we collected F4/80-positive cells from the stromal vascular fraction (SVF) of the eWAT using a magnetic activated cell sorting system and compared the mRNA expression (Fig. 7). Because

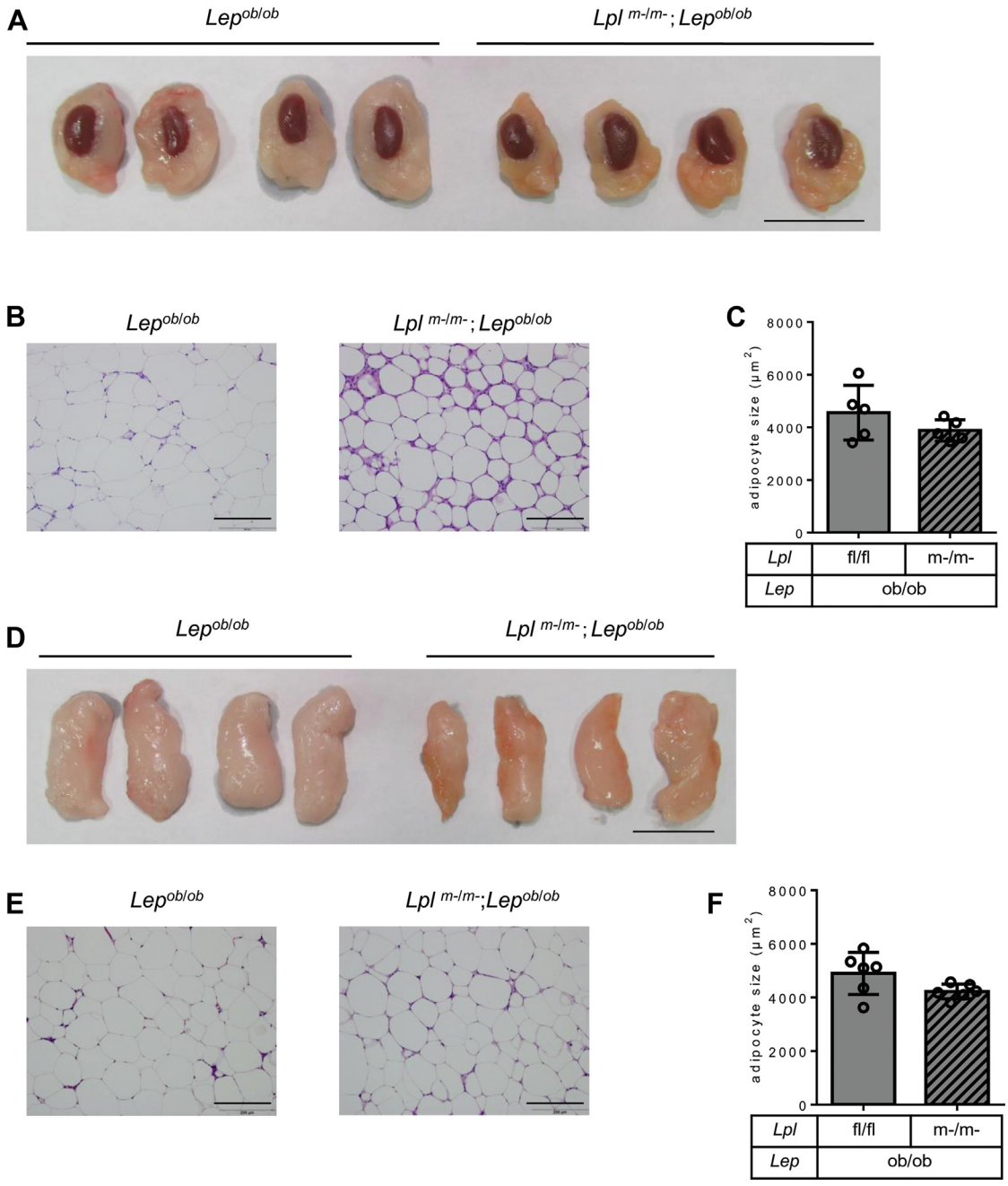

Figure 3. Gross appearance and histology of perirenal and subcutaneous adipose tissues. (*A, D*) perirenal and subcutaneous (inguinal) fats were taken from 24-week-old male mice for gross inspection. Two mice fat pads are shown in each genotype. The scale bar represents 2 cm. (*B, E*) H&E staining. The scale bar represents 200 μm. (*C, F*) the average adipocyte size was quantified (n = 5–6). Values are expressed as means ± SD.

the extensive fibrosis prohibited us to isolate SVF from 24-week-old $Lpl^{m-/m-}$;$Lep^{ob/ob}$ mice, we used 16-week-old mice whose fibrotic changes in the adipose tissue were milder (Fig. S1A). The eWAT mRNA expression levels of macrophage markers and the genes related to tissue fibrosis were essentially similar to those in eWAT of 24-week-old mice with some exceptions (Fig. S1, *B* and *C*): the expression of *F4/80* was increased, but the expression of *Timp1* and *Col6a3* was not increased in $Lpl^{m-/m-}$;$Lep^{ob/ob}$ mice compared with $Lep^{ob/ob}$ mice.

ATMs from $Lpl^{m-/m-}$;$Lep^{ob/ob}$ mice had negligible expression of *Lpl* mRNA compared with those from $Lep^{ob/ob}$ mice (Fig. 7*A*), confirming that ATMs were successfully isolated and that *Lpl* was successfully ablated in ATMs. The expression levels of genes related to tissue fibrosis (*Hif1a*, *Tgfb1,* and *Timp1*) were higher in ATMs from $Lpl^{m-/m-}$;$Lep^{ob/ob}$ compared with those from $Lep^{ob/ob}$ mice by 44%, 37%, and 91%, respectively (Fig. 7*D*). As had been noted in WAT, the expressions of M1 and M2 markers did not change in a constant manner (Fig. 7, *B* and *C*).

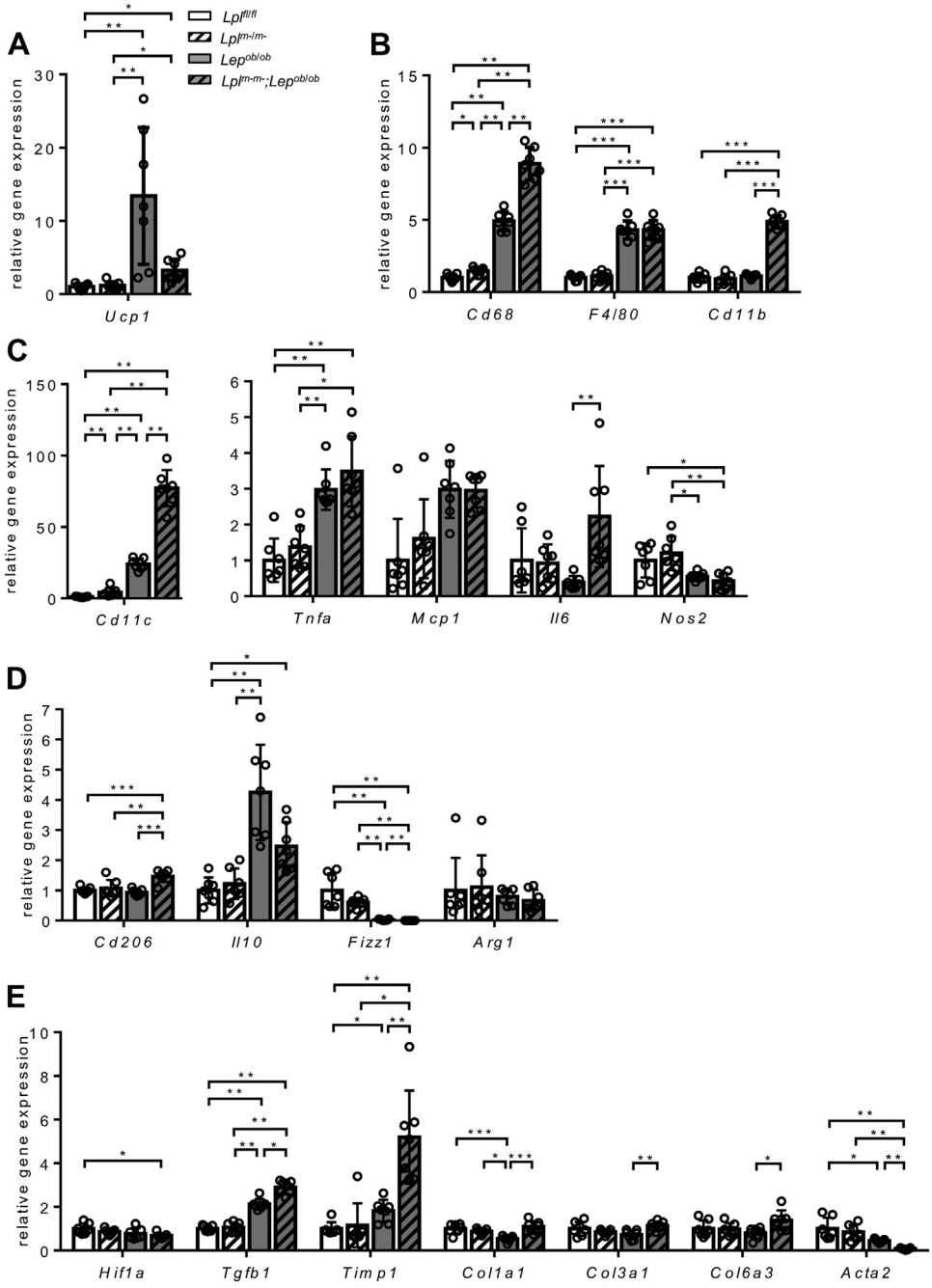

Figure 4. mRNA expression profiles in epididymal white adipose tissue. Total RNA was extracted from epididymal white adipose tissue of male mice with four genotypes at the age of 24 weeks. The mRNA expression levels were determined by real-time quantitative PCR. (*A*) *Ucp1*, (*B*) macrophage markers, (*C*) inflammatory M1 macrophage markers, (*D*) M2 macrophage markers, (*E*) tissue fibrosis related genes (n = 7). $Lpl^{fl/fl}$ (white bars), $Lpl^{m-/m-}$ (white hatched bars), $Lep^{ob/ob}$ (gray bars), $Lpl^{m-/m-};Lep^{ob/ob}$ (gray hatched bars). Values are expressed as means ± SD. * $p < 0.05$, ** $p < 0.01$, *** $p < 0.001$.

Despite the presence of greater numbers of necrotic cells (Fig. 2), the mRNA expression of the genes involved in efferocytosis, *Mer tyrosine kinase (MerTK)*, *Low-density lipoprotein receptor-related protein 1 (Lrp1),* and *growth arrest-specific 6* (*Gas6*), was higher in ATMs from $Lpl^{m-/m-};Lep^{ob/ob}$ compared with those from $Lep^{ob/ob}$ mice by 138%, 25%, and 181%, respectively (Fig. 7*E*). This suggests that greater gene expression was reactive, the receptors were not functional, or the creation of necrotic cells overwhelmed the uptake process.

$Lpl^{m-/m-};Lep^{ob/ob}$ *mice are more hypertriglyceridemic than* $Lep^{ob/ob}$ *mice*

To examine the effect of the loss of myeloid *Lpl* on glucose metabolism, we measured fasting blood glucose and insulin and calculated homeostasis model assessment of insulin resistance. $Lpl^{m-/m-};Lep^{ob/ob}$ mice had lower fasting blood glucose and homeostasis model assessment of insulin resistance than $Lep^{ob/ob}$ mice, suggesting that they were more insulin sensitive than $Lep^{ob/ob}$ mice (Table 1).

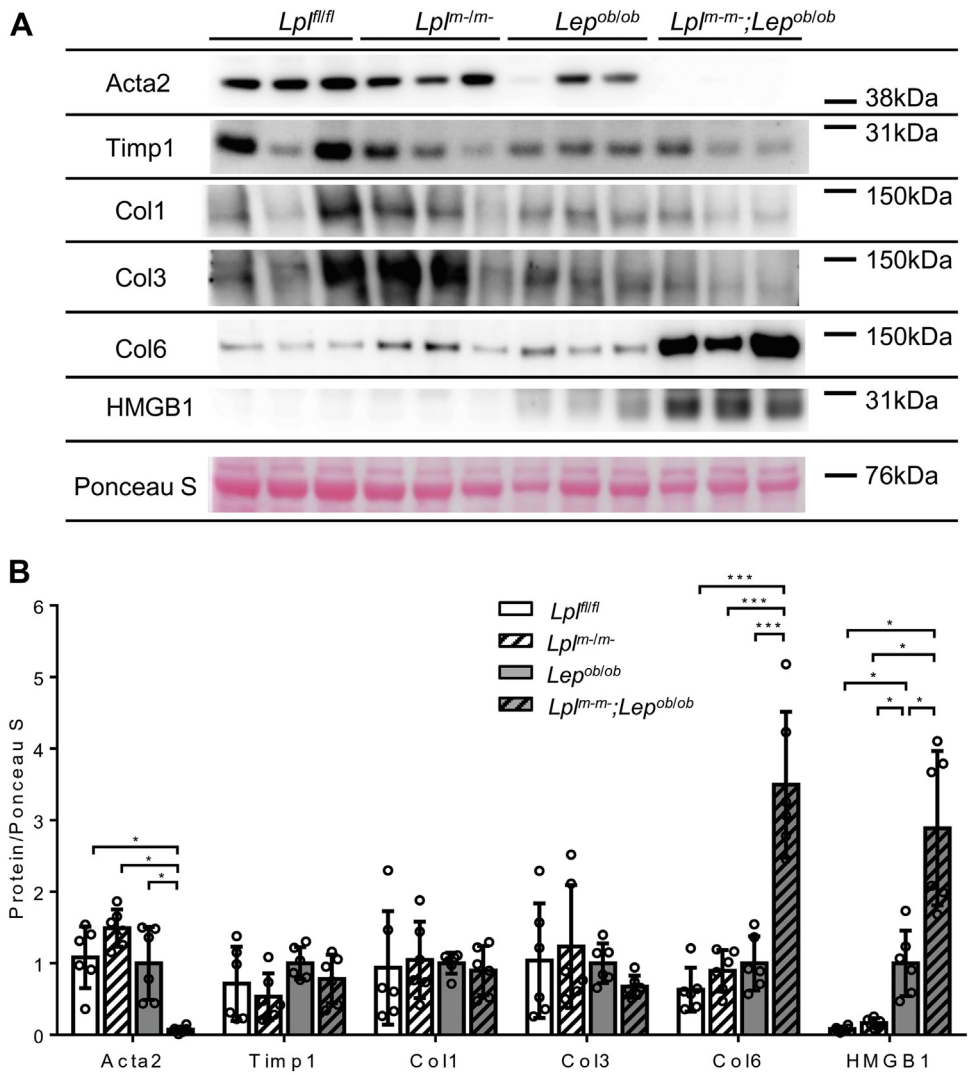

Figure 5. Protein expression profiles in epididymal white adipose tissue. Proteins were extracted from epididymal white adipose tissue of mice with four genotypes at the age of 24 weeks. Protein expression levels were determined by immunoblot analyses. (*A*) immunoblot analyses. (*B*) quantification of the immunoblot band density of each protein normalized to Ponceau S staining (n = 6). $Lpl^{fl/fl}$ (white bars), $Lpl^{m-/m-}$ (white hatched bars), $Lep^{ob/ob}$ (gray bars), $Lpl^{m-/m-};Lep^{ob/ob}$ (gray hatched bars). Values are expressed as means ± SD. * $p < 0.05$, *** $p < 0.001$.

To examine the effect of the loss of myeloid *Lpl* on plasma lipoprotein metabolism, we measured plasma levels of total cholesterol (TC), TG, and FFA (Table 1). $Lpl^{m-/m-};Lep^{ob/ob}$ mice had 2.1-fold higher levels of plasma TG than $Lep^{ob/ob}$ mice but 39% lower levels of plasma TC. The FFA levels were not different between the two groups. There were no significant differences in plasma levels of TC, TG, or FFA between $Lpl^{fl/fl}$ and $Lpl^{m-/m-}$ mice. As is known to occur with the *ob/ob* background, $Lep^{ob/ob}$ mice had 3.3-fold higher levels of plasma TC than $Lpl^{fl/fl}$ mice.

High-performance liquid chromatography (HPLC) analyses of plasma lipoproteins showed that VLDL-TG was increased (Fig. 8*B*) and low-density lipoprotein and high-density lipoprotein cholesterol were decreased (Fig. 8*A*) in $Lpl^{m-/m-};Lep^{ob/ob}$ mice compared with $Lep^{ob/ob}$ mice. LPL activity in post-heparin plasma was 45% less in $Lpl^{m-/m-};Lep^{ob/ob}$ mice than in $Lep^{ob/ob}$ mice (Fig. 8*C*). mRNA expression levels of *Lpl* in $Lpl^{m-/m-};Lep^{ob/ob}$ mice were 78% lower in eWAT, 45% lower in subcutaneous fat, and 37% lower in quadriceps than in $Lep^{ob/ob}$ mice (Fig. 8*D*). These results suggest that the reduced synthesis of macrophage-derived LPL in both adipose tissues and skeletal muscles contributed to the reduced activities of post-heparin lipolytic activity. Hepatic VLDL-TG production assessed by Triton WR1339 inhibition of lipolysis showed that production was increased in $Lpl^{m-/m-};Lep^{ob/ob}$ mice compared with that in $Lep^{ob/ob}$ mice (Fig. 8*E*). Therefore, both impaired clearance and overproduction of VLDL-TG contribute to the increased plasma level of VLDL-TG. To clarify how loss of *Lpl* increased hepatic VLDL production in *ob/ob* background, we measured mRNA expression of genes related to VLDL secretion (Fig. S2). There were no significant differences in the expression of the genes involved in VLDL secretion (*Mttp* or *Apob*), *de novo* lipogenesis (*Srebp1c*, *Fas,* and *Acc1*), or FFA β-oxidation (*Cpt1a* and *Acox1*). On the

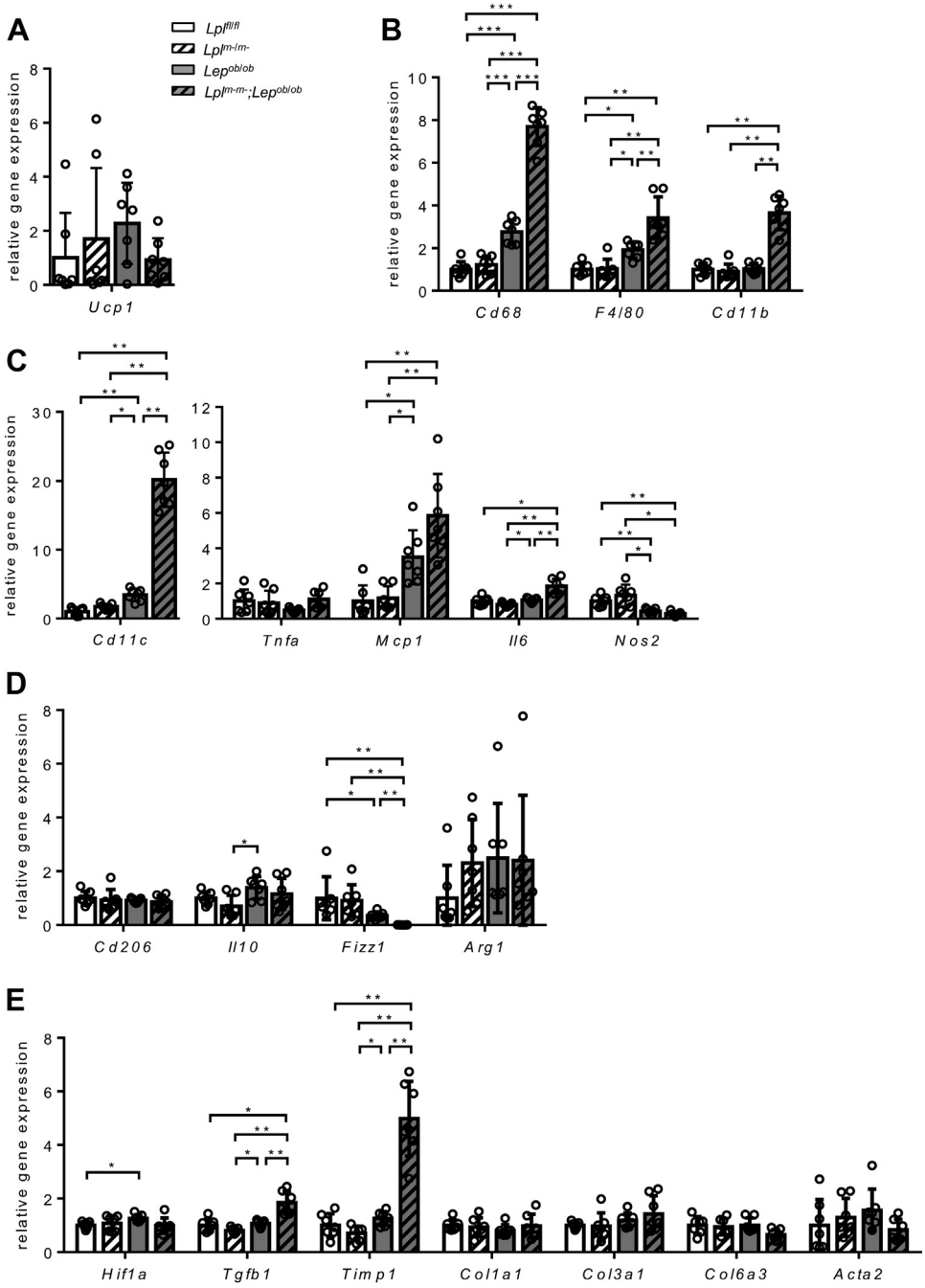

Figure 6. mRNA expression profiles in subcutaneous fat. Total RNA was extracted from subcutaneous fat of male mice with four genotypes at the age of 24 weeks. The mRNA levels were determined by real-time quantitative PCR. (*A*) *Ucp1*, (*B*) macrophage markers, (*C*) inflammatory M1 macrophage markers, (*D*) M2 macrophage markers, (*E*) tissue fibrosis related genes (n = 7). $Lpl^{fl/fl}$ (white bars), $Lpl^{m-/m-}$ (white hatched bars), $Lep^{ob/ob}$ (gray bars), $Lpl^{m-/m-}$;$Lep^{ob/ob}$ (gray hatched bars). Values are expressed as means ± SD. * $p < 0.05$, ** $p < 0.01$, *** $p < 0.001$.

contrary, the increased hepatic expression of *Lpl* in $Lep^{ob/ob}$ mice was abrogated in $Lpl^{m-/m-}$;$Lep^{ob/ob}$ mice.

Next, we evaluated hepatic steatosis (Fig. 8*F*). $Lep^{ob/ob}$ mice showed a 1.8-fold increase in hepatic TG content compared with $Lpl^{fl/fl}$ mice. There was no difference in hepatic TG content between $Lep^{ob/ob}$ and $Lpl^{m-/m-}$;$Lep^{ob/ob}$ mice. Consistently, there was no discernable difference in the pathological features of fatty liver disease such as ballooning of hepatocytes (Fig. S3A) and the extent of oil red O staining (Fig. S3B).

Loss of myeloid Lpl *reduces body weight in* $Lep^{ob/ob}$ *mice*

We measured body weight every week and weighed the organs at 24 weeks of age (Fig. 9, *A*–*D*). Both male and female $Lpl^{fl/fl}$ and $Lpl^{m-/m-}$ mice gained weight at similar rates over the entire observation period (Fig. 9, *A* and *B*). The weight of perigonadal, perirenal, mesenteric, and subcutaneous (inguinal) WAT was not different between the two groups (Fig. 9, *C* and *D*). $Lep^{ob/ob}$ mice gained significantly more weight than $Lpl^{fl/fl}$ and $Lpl^{m-/m-}$ mice throughout the study period (from 6 to 24 weeks of age) (Fig. 9, *A* and *B*). Beginning

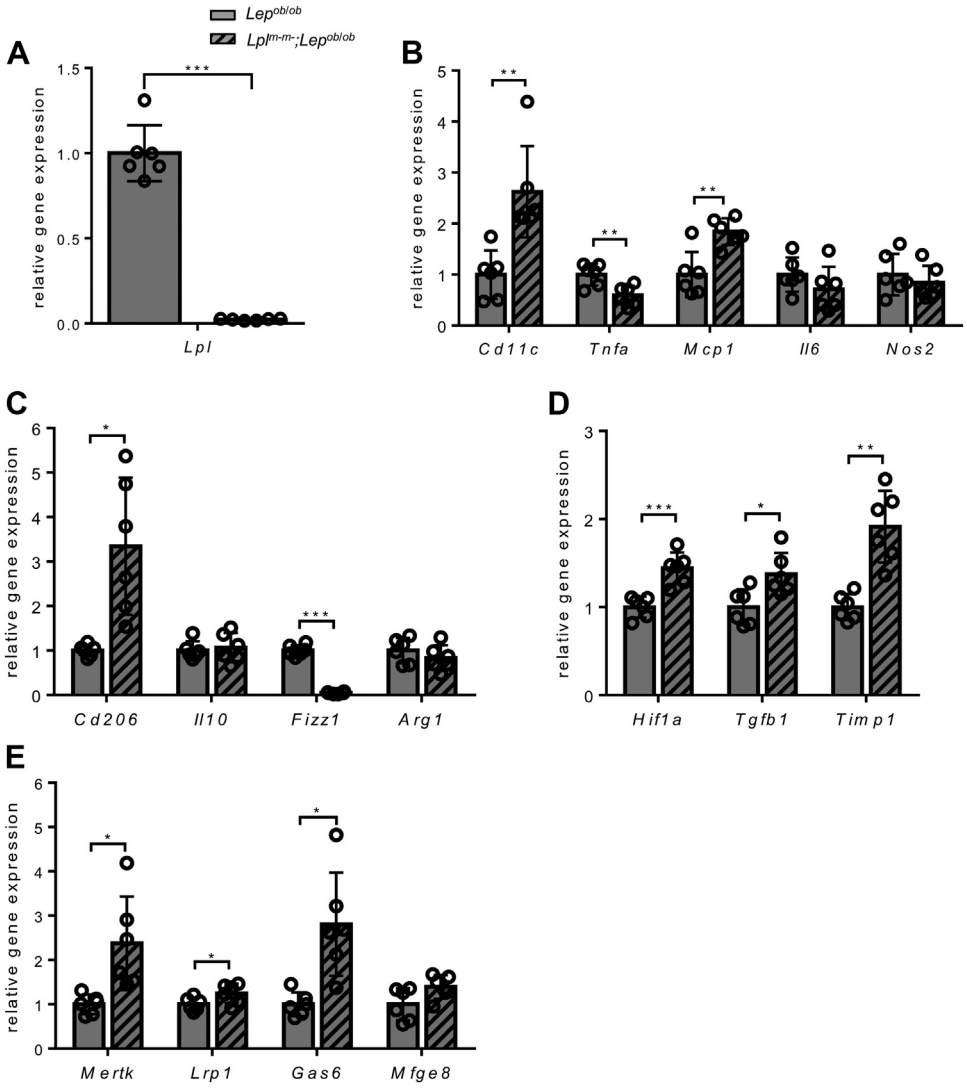

Figure 7. mRNA expression profiles in adipose tissue macrophages. F4/80-positive adipose tissue macrophages were collected from epididymal white adipose tissue of mice with two genotypes at the age of 16 weeks by magnetic sorting. The mRNA expression levels were determined by real-time quantitative PCR: (*A*) *Lpl*, (*B*) inflammatory M1 macrophage markers, (*C*) M2 macrophage markers, (*D*) tissue fibrosis-related genes, (*E*) efferocytosis-related genes (n = 6). $Lep^{ob/ob}$ (gray bars), $Lpl^{m-/m-}$;$Lep^{ob/ob}$ (gray hatched bars). Values are expressed as means ± SD.* $p < 0.05$, ** $p < 0.01$, *** $p < 0.001$.

at 15 to 16 weeks, both male and female $Lpl^{m-/m-}$;$Lep^{ob/ob}$ mice gained significantly less weight than $Lep^{ob/ob}$ mice. At the age of 24 weeks, $Lpl^{m-/m-}$;$Lep^{ob/ob}$ mice were 17% lighter than $Lep^{ob/ob}$ mice of the same sex (Fig. 9, *A* and *B*). $Lpl^{m-/m-}$;$Lep^{ob/ob}$ mice also had less subcutaneous fat than $Lep^{ob/ob}$ mice; the decrease was 34% in males and 28% in females. By contrast, $Lpl^{m-/m-}$;$Lep^{ob/ob}$ perigonadal fat pads (also termed eWAT in males) were 44% heavier than those from male

Table 1
Blood glucose and lipids

	$Lpl^{fl/fl}$	$Lpl^{m-/m-}$	$Lep^{ob/ob}$	$Lpl^{m-/m-}$;$Lep^{ob/ob}$
FBG (mmol/l)	2.94 ± 0.58	2.98 ± 0.56	6.64 ± 1.84[a]	4.99 ± 1.07[bc]
Insulin (ng/ml)	0.36 ± 0.28	0.24 ± 0.12	4.60 ± 2.30[a]	3.70 ± 0.64[d]
HOMA-IR	1.2 ± 0.8	0.8 ± 0.3	32.5 ± 10.4[a]	21.1 ± 4.8[dc]
ad lib BG (mmol/l)	6.63 ± 0.69	6.25 ± 0.87	8.70 ± 1.89[c]	6.16 ± 1.76[f]
Total cholesterol (mmol/l)	2.43 ± 0.25	2.26 ± 0.27	8.11 ± 0.87[a]	4.92 ± 0.80[dg]
Triglyceride (mmol/l)	1.01 ± 0.41	0.99 ± 0.41	1.44 ± 0.46	3.03 ± 1.81[bc]
FFA (mmol/l)	2.0 ± 0.2	1.8 ± 0.5	1.2 ± 0.3[a]	1.1 ± 0.1[d]

FBG, fasting blood glucose; HOMA-IR, homeostasis model assessment of insulin resistance.
Blood samples were collected after fasting for 16 h at the age of 22 to 24 weeks (n=7–11) or *ad libitum* fed (at the beginning of light cycle) mice at the age of 24 weeks (n=5–10). HOMA-IR was calculated as FBG (mg/dl) × fasting plasma insulin (μIU/ml) divided by 405.
[a] $p < 0.001$ compared with $Lpl^{fl/fl}$ mice.
[b] $p < 0.01$ compared with $Lpl^{m-/m-}$ mice.
[c] $p < 0.05$ compared with $Lep^{ob/ob}$ mice.
[d] $p < 0.001$ compared with $Lpl^{m-/m-}$ mice.
[e] $p < 0.05$ compared with $Lpl^{fl/fl}$ mice.
[f] $p < 0.01$ compared with $Lep^{ob/ob}$ mice.
[g] $p < 0.001$ compared with $Lep^{ob/ob}$ mice. Values are expressed as means ± SD.

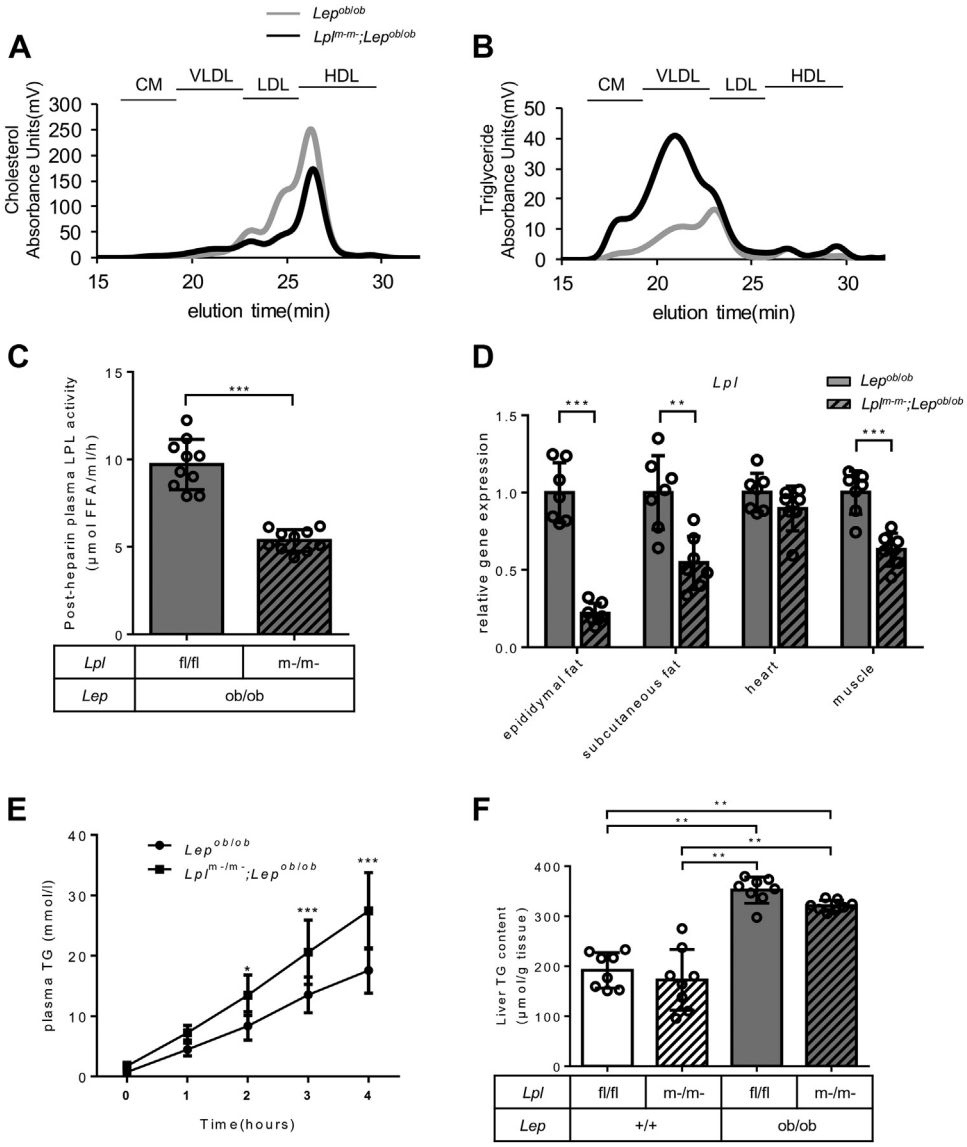

Figure 8. Lipoprotein metabolism in *Lep*$^{ob/ob}$ and *Lpl*$^{m-/m-}$;*Lep*$^{ob/ob}$ mice. Blood samples were collected after fasting for 16 h at the age of 24 weeks (*A, B*) pooled samples were analyzed by HPLC for *Lep*$^{ob/ob}$ (gray line) and *Lpl* $^{m-/m-}$;*Lep*$^{ob/ob}$ (black line) (n = 10–11). (*C*) post-heparin plasma lipoprotein lipase (LPL) activity (n = 10). (*D*) gene expression of *Lpl* in epididymal white adipose tissue, subcutaneous fat, heart, and quadriceps (n = 7). *Lep*$^{ob/ob}$ (gray bars), *Lpl*$^{m-/m-}$;*Lep*$^{ob/ob}$ (gray hatched bars). (*E*) hepatic very-low-density lipoprotein production after injection of Triton WR1339 (n = 8 for *Lep*$^{ob/ob}$ and n = 7 for *Lpl*$^{m-/m-}$;*Lep*$^{ob/ob}$ mice). (*F*) liver triglyceride (TG) content (n = 8). Values are expressed as means ± SD. * $p < 0.05$, ** $p < 0.01$, *** $p < 0.001$.

Lep$^{ob/ob}$ mice, while they were 34% heavier in females. There were no significant differences in the weight of mesenteric fat, brown adipose tissue, and liver between the two groups (Fig. 9, *C* and *D*). Computed tomography (CT) scan of the whole bodies revealed that subcutaneous fat mass was decreased in *Lpl*$^{m-/m-}$;*Lep*$^{ob/ob}$ mice compared with *Lep*$^{ob/ob}$ mice by 42% (Fig. S4). However, visceral fat mass was not different between the two groups. Therefore, the smaller gain of body weight in *Lpl*$^{m-/m-}$;*Lep*$^{ob/ob}$ mice can be ascribed to the smaller weight gain in subcutaneous fat.

Lpl$^{m-/m-}$;Lep$^{ob/ob}$ *mice eat less food than* Lep$^{ob/ob}$ *mice*

To understand why *Lpl*$^{m-/m-}$;*Lep*$^{ob/ob}$ mice were lighter than *Lep*$^{ob/ob}$ mice, we measured food intake, core body temperatures, energy expenditure, and locomotor activity (Fig. 9, *E–I*). Cumulative food intake was not different between *Lpl*$^{fl/fl}$ and *Lpl*$^{m-/m-}$ mice (Fig. 9*E*). However, cumulative food intake in *Lpl*$^{m-/m-}$;*Lep*$^{ob/ob}$ mice was significantly reduced from 19 weeks of age compared with intake by *Lep*$^{ob/ob}$ mice (Fig. 9*E*). Daily food consumption, which was calculated from the food intake from 9 to 24 weeks of age, was reduced by 11% in *Lpl*$^{m-/m-}$;*Lep*$^{ob/ob}$ mice compared with *Lep*$^{ob/ob}$ mice (Fig. 9*F*). Core body temperatures were not different between *Lep*$^{ob/ob}$ and *Lpl*$^{m-/m-}$;*Lep*$^{ob/ob}$ mice (35.4 ± 0.8°C *versus* 35.2 ± 0.7°C, n=8–10). Oxygen consumption (VO_2) and carbon dioxide production (VCO_2) during light, dark, and 24-h periods and locomotor activity were not different between the two groups at 9 to 10 and 23 weeks of age (Fig. 9, *G–I*). The results were essentially the same when the data were analyzed for light

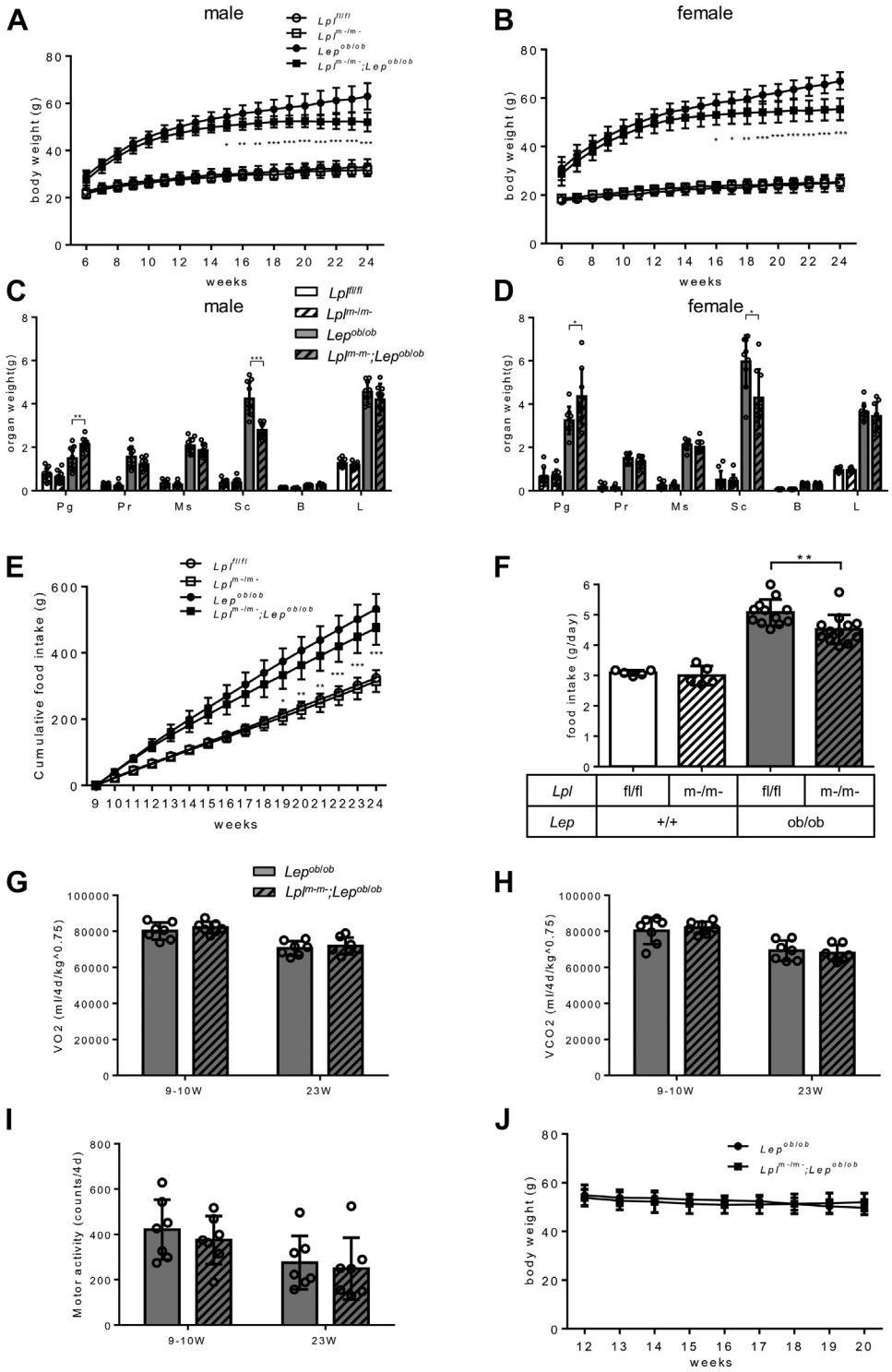

Figure 9. Loss of myeloid *Lpl* attenuates weight gain of body and subcutaneous adipose tissues and reduces food intake in *Lep*$^{ob/ob}$ mice. (*A, B*) Body weight of male and female mice was measured weekly from 6 to 24 weeks (n=9–11). (*C, D*) fat weights and liver weights of male and female mice were measured at 24 weeks of age after overnight fast. Pg, perigonadal white adipose tissue (WAT); Pr, perirenal WAT; Ms, mesenteric WAT; Sc, subcutaneous (inguinal) WAT; B, brown adipose tissue; L, liver. (*E, F*) cumulative food intake and daily food intake of female mice were calculated by weekly food intake after the mice were housed in an individual cage from 9 to 24 weeks old (n = 5 for *Lpl*$^{fl/fl}$and *Lpl*$^{m-/m-}$, n = 12 for *Lep*$^{ob/ob}$ and *Lpl*$^{m-/m-}$;*Lep*$^{ob/ob}$ mice). (*G*) VO_2, (*H*) VCO_2, and (*I*) motor activity of female mice were measured at the age of 9 to 10 (n = 7) and 23 weeks (n = 7) for 4 days. (*J*) body weight changes of female mice during a pair feeding experiment from 12 to 20 weeks old (n = 4). *Lpl*$^{fl/fl}$ (open circle, white bars), *Lpl*$^{m-/m-}$ (open square, white hatched bars), *Lep*$^{ob/ob}$ (closed circle, gray bars), *Lpl* $^{m-/m-}$;*Lep*$^{ob/ob}$ (closed square, gray hatched bars). Values are expressed as means ± SD. *$p < 0.05$, **$p < 0.01$, ***$p < 0.001$, *versus Lep*$^{ob/ob}$ mice.

and dark phases separately (Fig. S5). In a pair feeding experiment, we did not find a significant difference in the changes of body weight when fed the same amount of diet (4.3 g) every day for 8 weeks from 12 to 20 weeks of age (Fig. 9*J*), supporting that the difference in the body weight gain reflected the difference in food intake but not that in energy expenditure.

We explored the reasons for the change in eating. Expression of orexigenic neuropeptides *neuropeptide Y (Npy)* and *Agouti-related peptide (Agrp)*, which were increased in $Lep^{ob/ob}$ mice compared with $Lpl^{fl/fl}$ mice, were not different between $Lpl^{m-/m-}$;$Lep^{ob/ob}$ and $Lep^{ob/ob}$ mice (Fig. S6). The expression of *pro-opiomelanocortin (Pomc)*, an anorexigenic neuropeptide, which was reduced in $Lep^{ob/ob}$ mice compared with $Lpl^{fl/fl}$ mice, was also not different between $Lpl^{m-/m-}$;$Lep^{ob/ob}$ and $Lep^{ob/ob}$ mice (Fig. S6).

Discussion

In the present study, we investigated the effects of the loss of *Lpl* in myeloid cells on the morphology and gene expression in the WAT and other obesity-related phenotypes in a $Lep^{ob/ob}$ background. The most striking phenotypes were worsening of interstitial fibrosis with Col6 deposition and increased infiltration of ATMs with both proinflammatory and anti-inflammatory characteristics, which surrounded perilipin-negative (dead) adipocytes and disappearance of Acta 2 expression in the perigonadal WAT, but not in the subcutaneous WAT. We also found that $Lpl^{m-/m-}$;$Lep^{ob/ob}$ mice had hypertriglyceridemia likely due to both reduced LPL activity and increased VLDL production, and decreased overall adiposity conceivably due to the decreased food intake.

First, we would like to discuss the phenotype in the WAT. The eWAT of $Lpl^{m-/m-}$;$Lep^{ob/ob}$ mice contained substantial amounts of necrotic adipocytes (Fig. 2), as detected by perilipin-negative lipid droplets, with an increase in the number of ATMs, and extensive fibrosis detected using Masson's trichrome and Sirius red staining (Fig. 1, *E–H*). The mRNA expression patterns of the eWAT from 24-week-old mice were largely consistent with the pathology. The loss of *Lpl* upregulated some of M1 (*Cd11c*) and M2 markers (*Cd206* and *Tgfb1*) (Fig. 4, *B–D*). Concomitantly, genes related to fibrosis (*Timp1*, *Col1a1*, *Col3a1,* and *Col6a3*) increased (Fig. 4*E*). The changes in *Cd11c, Cd206, Fizz1, Tgfb1,* and *Timp1* in the eWAT were also observed in the ATMs (Fig. 7). It is of note that some M2 markers were decreased (*Fizz1*) or unchanged (*Arg1*). In general, M2 macrophages are thought to be associated with fibrosis (26). Although we did not confirm these findings in flow cytometric analysis, which was difficult to perform because of the extensively fibrotic eWAT, we could conclude that the loss of *Lpl* polarized the ATMs toward both proinflammatory M1 (*Cd11c*) and anti-inflammatory M2 phenotypes (*Cd206* and *Tgfb1*). Probably, M1 and M2 phenotypes are not mutually exclusive, as exemplified by adipose tissues that have both CD11c and CD206 in obese humans (27), and M2-like $CD11c^{+}$ ATMs in obese mice (28).

In support of the results of mRNA expression, the protein contents of Col6, but not Timp1, Col1, and Col3, were significantly increased in the eWAT of $Lpl^{m-/m-}$;$Lep^{ob/ob}$ mice compared with that of $Lep^{ob/ob}$ mice (Fig. 5). The remarkable accumulation of Col6 might have resulted from both increased synthesis and decreased degradation due to the increased Timp1, an inhibitor of many matrix metalloproteinases. The amounts of Col6 in WAT are reported to be correlated with WAT fibrosis, inflammation, and insulin resistance in mice (29) and humans (30, 31). Since leptin is known to inhibit Col6a3 expression (32), its deficiency might accentuate the Col6 overproduction, leading to WAT fibrosis in the current model of *ob/ob* background. However, a similar extensive fibrosis with Col6 deposition was observed in eWAT of $Lpl^{m-/m-}$ mice fed a high-fat diet containing 60 kcal% fat for 24 weeks (data not shown), indicating that obesity itself exacerbated WAT fibrosis in $Lpl^{m-/m-}$ mice irrespective of the presence of leptin signaling.

In adipose tissue, collagens are synthesized by various cell types such as adipocyte progenitors, adipocytes, fibroblasts, and myofibroblasts (4). mRNA and protein expressions of Acta2 were significantly reduced in the eWAT of $Lpl^{m-/m-}$;$Lep^{ob/ob}$ mice compared with that of $Lep^{ob/ob}$ mice (Fig. 4*E* and 5). Consistently, Jager *et al.* reported a similar decrease in the expression of Acta2 in SVF from fibrotic eWAT of mice fed a high-fat diet compared with that from mice fed a low-fat diet (33). Since Acta2 is normally expressed in myofibroblasts (24) or platelet-derived growth factor receptor-α-positive adipocyte progenitors (34), it is unlikely that an increase in the number of these cells mediated the fibrosis in the eWAT of $Lpl^{m-/m-}$;$Lep^{ob/ob}$ mice. Together with the finding that Col6, which is specifically secreted by adipocytes (29), is significantly increased in the eWAT of $Lpl^{m-/m-}$;$Lep^{ob/ob}$ mice (Fig. 5), it is more conceivable that adipocytes are the origin of the accumulated collagens.

It is of note that adipose tissue fibrosis was not observed in $Apoe^{-/-}$ mice lacking myeloid *Lpl* ($Lpl^{m-/m-}$;$Apoe^{-/-}$) fed Western-type diet for 12 weeks in our preceding study (14). It is possible that the obesity attained by feeding Western-type diet for 12 weeks was not sufficient to cause adipose tissue fibrosis due to resistance to obesity of $Apoe^{-/-}$ mice (23). Another possible explanation is that changes in white blood cells due to leptin deficiency (35) or greatly accelerated adipose development promotes fibrosis when these changes are combined with the effects of *Lpl* deficiency.

The ATMs from $Lpl^{m-/m-}$;$Lep^{ob/ob}$ mice showed high expression of efferocytosis-related molecules compared with the ATMs from $Lep^{ob/ob}$ mice (Fig. 7*E*). Similar upregulation of the efferocytosis-related genes was reported in mice deficient in mannose-binding lectin (36). These mice had an increased number of crown-like structures and apoptotic cells in adipose tissue due to defective clearance of dying adipocytes, together with enhanced expression of efferocytosis-related molecules. It is interesting to note that macrophage LPL enhanced Fc receptor-mediated phagocytosis especially under low glucose conditions *in vitro* (9). Indeed, LPL is a ligand for low-density lipoprotein receptor-related protein 1 (LRP1), which is an efferocytosis-related molecule (37). These results suggest that LPL in ATMs is required for the effective clearance of apoptotic cells, which, in this case, would be dying adipocytes. It is conceivable that the dying adipocytes induce ATM efferocytosis pathways, but the clearance inefficiency caused by LPL deficiency leads to release of alarmins or damage-associated molecular patterns such as HMGB1, which subsequently stimulate tissue fibrosis (38). Indeed, HMGB1 protein

content was markedly increased in the eWAT of $Lpl^{m-/m-}$;$Lep^{ob/ob}$ mice (Fig. 5). Although it is not known whether the accumulated HMGB1 is originated from undisposed dead adipocytes or from stimulated adipocytes and/or immune cells, it is reasonable to speculate that the HMGB1 accumulated in WAT stimulates fibrosis and inhibits efferocytosis of the dead adipocytes.

How did the loss of *Lpl* change the phenotype of ATMs? Fatty acids produced by lipolysis stimulate the expression of some pro- or anti-inflammatory markers in macrophages (39, 40). Moreover, M1 macrophages depend on glycolysis and oxidative phosphorylation of pyruvate, while M2 macrophages depend on fatty acid oxidation (41). Therefore, loss of *Lpl* might modulate macrophage phenotype by restricting the supply of fatty acids. Moreover, the alarmins produced from dying adipocytes might make the ATMs more fibrogenic, as discussed above.

LPL expressed in myocytes and adipocytes is thought to be responsible for regulation of circulating TG levels. For this reason, we did not expect $Lpl^{m-/m-}$;$Lep^{ob/ob}$ mice to have higher level of TG (Table 1) and VLDL (Fig. 8*B*). Because the LPL activity in the post-heparin plasma was decreased (Fig. 8*C*), the impaired clearance of VLDL likely contributed to the hypertriglyceridemia. In the eWAT and subcutaneous fat, the mRNA expression of *Lpl* was significantly decreased. This might reflect either the reduction in macrophage or adipose LPL expression. Given that ATMs comprise as much as 50% of cells in adipose tissue in severe obesity (20), loss of *Lpl* in ATMs likely contributes to the reduced *Lpl* expression in the WAT. However, the immunostaining for perilipin suggested most of the adipocytes were not alive in the eWAT of $Lpl^{m-/m-}$;$Lep^{ob/ob}$ mice (Fig. 2). Therefore, reduction of LPL secretion from adipocytes might also contribute to the reduced *Lpl* expression in the WAT. Skeletal muscle also contains macrophages whose numbers are increased with obesity (42). Therefore, it is possible that macrophages are also responsible for the reduced *Lpl* in muscle. In addition to the impaired clearance of VLDL, VLDL overproduction might contribute to the hypertriglyceridemia. Because there were not significant differences in plasma NEFA levels and the gene expression of VLDL assembly, *de novo* lipogenesis, and FFA β-oxidation, it is unlikely that VLDL secretion rate per hepatocyte was increased. We would rather ascribe the reduced hepatic expression of *Lpl* due to the lack of LPL secretion from hepatic macrophages, which are increased in *ob/ob* mice, to the VLDL overproduction.

Finally, we would like to discuss the obesity-related phenotype. How did the loss of myeloid *Lpl* decrease body weight gain and food intake in the setting of leptin deficiency? We previously reported that body weight of $Apoe^{-/-}$ mice lacking myeloid *Lpl* ($Lpl^{m-/m-}$;$Apoe^{-/-}$) fed Western-type diet for 12 weeks and $Lpl^{m-/m-}$ mice fed a high-fat diet containing 45 kcal% fat for 10 weeks were not different from that of control groups (14). This initially suggested that leptin deficiency led to the reduction of body weight of $Lpl^{m-/m-}$;$Lep^{ob/ob}$ mice. Since there were no differences in energy expenditure, locomotor activity, and body weight gain in a pair feeding experiment, the attenuation of body weight gain in $Lpl^{m-/m-}$;$Lep^{ob/ob}$ mice should be attributable to the reduced food intake. Interestingly, similar attenuation of body weight gain was observed in $Lep^{ob/ob}$ mice lacking hormone-sensitive lipase (*Lipe*) globally (43).

Because lysozyme is expressed in the brain cells such as microglia and neurons (44), it is possible that loss of *Lpl* in these cells modulated the appetite. Although deletion of *Lpl* in neurons under the control of NEX (MATH2, NeuroD6) made mice hyperphagic and obese (45), deletion of *Lpl* in microglia might have an opposite effect on appetite via modulating the activation status of microglia (46). Further studies are warranted to clarify the underlying mechanism.

In conclusion, the loss of myeloid *Lpl* led to extensive fibrosis of perigonadal WAT, hypertriglyceridemia, and reduced food intake in leptin-deficient mice. Moreover, we show that macrophage LPL assists in modulating circulating TG levels under conditions of metabolic stress. Increased adipose content of dead adipocytes suggests that, in some tissues, macrophage LPL is needed for efficient efferocytosis. Greater adipocyte synthesis of Col6 in mice deficient in both LPL and leptin suggests a secondary fibrotic response to impaired clearance of dead cells. These results should advance our understanding of the mechanisms by which ATMs control adipose tissue fibrosis in obesity and illustrate additional functions for LPL exclusive of lipid uptake.

Experimental procedures

The mice and antibodies used for the experiments were summarized in Table S1.

Mice

All animal experiments were approved by the Institutional Animal Care and Research Advisory Committee at Jichi Medical University. $Lpl^{m-/m-}$ mice were generated by crossing floxed *Lpl* mice (47) with transgenic mice on a C57BL/6J background in which Cre recombinase was expressed in myeloid cells under the control of the lysozyme promotor (Lys–Cre) (Jackson Laboratory) (14). Thereafter, $Lpl^{m-/m-}$ mice were crossbred with mice heterozygous for leptin deficiency to generate $Lpl^{m-/-}$;$Lep^{ob/ob}$ mice, which were then recrossed to produce $Lpl^{m-/m-}$;$Lep^{ob/ob}$ and $Lep^{ob/ob}$ littermates. Mice were fed a normal laboratory diet containing 4.8% (w/w) fat and 25.1% (w/w) protein (CE-2, Japan CLEA). All mice were maintained at controlled temperature (23°C) and humidity (50%) under a light 12 h/dark 12 h cycle in a room kept under a condition equivalent to specific pathogen free and given free access to food. No criteria except for age, gender, and genotypes were set for inclusion and exclusion. Mice were randomly assigned to each experimental group from littermates. If necessary, the mice were euthanized by cervical dislocation. All efforts were made to minimize potential cofounders and suffering.

M.T. was aware of group allocation. No adverse events were observed during the study period.

CT scans

The body fat composition was analyzed by CT scans using LaTheta LCT-200 (Hitachi Aloka Medical) and LaTheta software (Hitachi Aloka Medical) according to the manufacture's protocol. Anesthetized mice were scanned at 1-mm intervals from nose to anus.

Food intake

Weekly food intake and body weight of female mice were measured after the mice were housed in an individual cage at 9 weeks of age.

Pair-feeding experiment

Based on the results of food intake, we calculated the average daily food intake from 12 to 20 weeks to be 4.3 g. We fed that amount of food every day for 8 weeks as described (48).

Locomotor activity and indirect calorimetry

After female mice were acclimated in an individual metabolic cage for 3 days, VO_2 and VCO_2 were measured using ARCO-2000 (ARCO System) for 4 days as described (49). Locomotor activity was measured using the ACTIMO-100 activity monitoring system (Shinfactory). The mice were used at 9 to 10 and 23 weeks of age.

Measurements of glucose, insulin, lipids, and lipoproteins

Blood glucose was determined by a FreeStyle blood glucose monitoring system (NIPRO). Plasma insulin was determined by mouse ELISA kits (Morinaga). TC, TG, and FFA concentrations were determined enzymatically using Determiner L TCII (Kyowa Medex), L-Type Wako TG M (Fujifilm), and NEFA C-test Wako (Fujifilm). Plasma lipoproteins were analyzed by HPLC (50). After the lipids were extracted from the liver and eWAT by methanol and chloroform, TG contents were measured with an enzymatic kit.

Measurements of LPL activity

Plasma was obtained 10 min after 300 U/kg of heparin was intravenously injected to the fasted mice for measurements of LPL activity in triplicates (14).

Measurements of VLDL-TG production

Hepatic VLDL-TG production was estimated by intravenous injection of 500 mg/kg of Triton WR1339 (50). Plasma TG concentrations were measured at 1, 2, 3, and 4 h after injection.

Histology

The tissues of 24-week-old mice were fixed with 4% paraformaldehyde. Frozen sections of the liver were stained with Oil red O. Paraffin-embedded sections of the adipose tissue and liver were stained with hematoxylin and eosin, Masson's trichrome, or Sirius red. More than 200 cells were analyzed for determination of the average adipocyte size using ImageJ software (National Institutes of Health). Masson's trichrome– or Sirius red–positive areas were used to estimate the extent of fibrosis. For immunofluorescence, sections were incubated with Mac-2 antibody (Cedarlane) and perilipin antibody (Sigma-Aldrich) overnight. The sections were incubated with Alexa Fluor 488 (Thermo Fisher Scientific) for Mac-2 and/or Alexa Fluor 568 (Thermo Fisher Scientific) for perilipin. Nucleus was stained with 4′,6-diamidino-2-phenylindole (DAPI). Images of sections were captured using a confocal laser microscope (FV1000; Olympus). Perilipin staining was used to identify necrotic adipocytes. More than 400 cells were analyzed for determination of the necrotic adipocytes.

Collagen content in adipose tissue

Collagen content in adipose tissue was measured with a collagen assay kit (QuickZyme Biosciences).

Isolation of F4/80-positive cells by magnetic sorting

F4/80-positive cells were isolated from the SVF of eWAT of male mice using MS columns (Miltenyi Biotec) for magnetic activated cell sorting system (51).

Measurements of mRNA by real-time quantitative PCR

mRNA was measured by real-time quantitative PCR using mouse *Actb* mRNA as an invariant control as described (51). The primer-probe sets for real-time quantitative PCR are listed in Table S2.

Immunoblot analyses

Aliquots of frozen eWAT (∼150 mg) were homogenized in 200 μl of a buffer (50 mM Tris-HCl at pH 7.4, 150 mM NaCl, 2 mM sodium EDTA, 1% NP-40) supplemented with a protease inhibitor cocktail (Sigma). Protein, 30 μg. was subjected to 3 to 8% SDS-PAGE for immunoblot analyses of collagen I(Col1), Col3, and Col6 or 10% SDS-PAGE for immunoblot analyses of Acta2, Timp1, and HMGB1. After the membranes were blocked for 30 min in a blocking one solution (Nacalai Tesque), they were incubated with primary antibodies for Timp1 (R&D systems), Col1 (Bioss), Col3 (Bioss), Col6 (Novus Biologicals), Acta2 (abcam), or HMGB1 (abcam) overnight at 4°C. The membranes were incubated with anti-rabbit (GE healthcare) or anti-goat (Proteintech) IgG horseradish peroxidase–conjugated secondary antibody for 1 h in TBS-T solution at room temperature. An enhanced chemiluminescent substrate ECL prime (GE Healthcare) was used to visualize the horseradish peroxidase. Image Quant Las 4000mini (Cytiva) was used to detect the enhanced chemiluminescence. All membranes were stained with Ponceau S after protein transfer for protein normalization.

Statistics

Data are presented as means ± SD. GraphPad Prism version 6.0 (GraphPad Software) and EZR version 1.52 (Saitama Medical Center, Jichi Medical University), graphical user interface for R version 4.02 (R Foundation for Statistical

Computing), were used for data analyses. The Shapiro–Wilk test was used to test normality; F or Brown–Forsythe test was used to test equal variance. If the data were consistent with normal distribution and equal variance, Student's t test was used to compare the mean values between two groups, and the one-way ANOVA was used for multiple comparison. If the variances were not equal, Welch t test was used for comparison between two groups. When ANOVA results were statistically significant (*i.e.*, $p < 0.05$), individual comparisons were made with the Tukey post hoc test. If the data were not distributed normally, nonparametric tests such as the Mann–Whitney U or Kruskal–Wallis test were used. When Kruskal–Wallis test results were statistically significant (*i.e.*, $p < 0.05$), individual comparisons were made with the Steel–Dwass post hoc test. Body weights were compared by repeated-measures ANOVA with Bonferroni's post hoc analysis.

Data availability

The data that support the findings of this study are available from the corresponding authors upon reasonable request.

Supporting information—This article contains supporting information.

Acknowledgments—The authors thank Mika Hayashi, Nozomi Takatsuto, and Mihoko Sejimo for excellent technical support. The authors also thank Biopathology Institute Co, Ltd for helping to perform histological analyses.

Author contributions—M. T., S. I. conceptualization; M. T. methodology; M. T. formal analysis; M. T., D. Y., Y. T. investigation; H. Y., I. J. G. resources; M. T., S. I. writing – original draft; H. Y., D. Y., Y. T., I. J. G., T. O., T. W., A. T., S. T., S. N., H. O., K. E. writing – review & editing; M. T., D. Y., Y. T. visualization; S. I., H. Y., T. O. supervision; S. I. project administration; M. T., S. I. funding acquisition.

Funding and additional information—This study was supported by Grants-in-Aid for Scientific Research (JSPS KAKENHI Grant Number JP16K21318), Non-communicable diseases from the Ministry of Education, Culture, Sports, Science, and Technology of Japan, Jichi Medical University Young Investigator Award (for M. T.) and unrestricted grants from Astellas Pharma, Daiichi Sankyo Co, Shionogi Co, Boehringer Ingelheim Japan, Kowa, Co, Ono Pharma, Mitsubishi Tanabe Pharma, Takeda Pharma Co, Toyama Chemical Co, Teijin, Sumitomo Dainippon Pharma, Sanofi K.K., Novo Nordisk Pharma, MSD K.K., Pfizer Japan, Novartis Pharma, and Eli Lilly Co. I. J. G. is supported by grants HL45095 and 73029 from the NHLBI, National Institutes of Health (USA). The content is solely the responsibility of the authors and does not necessarily represent the official views of the National Institutes of Health.

Conflict of interest—The authors declare that they have no conflicts of interest with the contents of this article.

Abbreviations—The abbreviations used are: Arg1, (arginase 1); ATMs, (adipose tissue macrophages); Col, (collagen); CT, (computed tomography); eWAT, (epididymal white adipose tissue); FFA, (free fatty acids); HMGB1, (high-mobility group box 1); LPL, (lipoprotein lipase); $Lep^{ob/ob}$, (mice lacking leptin); $Lpl^{fl/fl}$, (mice with floxed *Lpl*); $Lpl^{m-/m-}$, (mice lacking lipoprotein lipase in myeloid cells); SVF, (stromal vascular fraction); TC, (total cholesterol); TG, (triglyceride); Timp1, (tissue inhibitor of metalloproteinase 1); VLDL, (very low-density lipoprotein); WAT, (white adipose tissue).

References

1. Crewe, C., An, Y. A., and Scherer, P. E. (2017) The ominous triad of adipose tissue dysfunction: Inflammation, fibrosis, and impaired angiogenesis. *J. Clin. Invest.* **127**, 74–82
2. Cinti, S., Mitchell, G., Barbatelli, G., Murano, I., Ceresi, E., Faloia, E., *et al.* (2005) Adipocyte death defines macrophage localization and function in adipose tissue of obese mice and humans. *J. Lipid Res.* **46**, 2347–2355
3. McNelis, J. C., and Olefsky, J. M. (2014) Macrophages, immunity, and metabolic disease. *Immunity* **41**, 36–48
4. Datta, R., Podolsky, M. J., and Atabai, K. (2018) Fat fibrosis: Friend or foe? *JCI Insight* **3**, e122289
5. Halberg, N., Khan, T., Trujillo, M. E., Wernstedt-Asterholm, I., Attie, A. D., Sherwani, S., *et al.* (2009) Hypoxia-inducible factor 1alpha induces fibrosis and insulin resistance in white adipose tissue. *Mol. Cell Biol.* **29**, 4467–4483
6. Martinez-Santibanez, G., and Lumeng, C. N. (2014) Macrophages and the regulation of adipose tissue remodeling. *Annu. Rev. Nutr.* **34**, 57–76
7. Morinaga, H., Mayoral, R., Heinrichsdorff, J., Osborn, O., Franck, N., Hah, N., *et al.* (2015) Characterization of distinct subpopulations of hepatic macrophages in HFD/obese mice. *Diabetes* **64**, 1120–1130
8. Olivecrona, G. (2016) Role of lipoprotein lipase in lipid metabolism. *Curr. Opin. Lipidol.* **27**, 233–241
9. Yin, B., Loike, J. D., Kako, Y., Weinstock, P. H., Breslow, J. L., Silverstein, S. C., *et al.* (1997) Lipoprotein lipase regulates Fc receptor-mediated phagocytosis by macrophages maintained in glucose-deficient medium. *J. Clin. Invest.* **100**, 649–657
10. Ishibashi, S., Yamada, N., Shimano, H., Mori, N., Mokuno, H., Gotohda, T., *et al.* (1990) Apolipoprotein E and lipoprotein lipase secreted from human monocyte-derived macrophages modulate very low density lipoprotein uptake. *J. Biol. Chem.* **265**, 3040–3047
11. Obunike, J. C., Edwards, I. J., Rumsey, S. C., Curtiss, L. K., Wagner, W. D., Deckelbaum, R. J., *et al.* (1994) Cellular differences in lipoprotein lipase-mediated uptake of low density lipoproteins. *J. Biol. Chem.* **269**, 13129–13135
12. Babaev, V. R., Fazio, S., Gleaves, L. A., Carter, K. J., Semenkovich, C. F., and Linton, M. F. (1999) Macrophage lipoprotein lipase promotes foam cell formation and atherosclerosis *in vivo*. *J. Clin. Invest.* **103**, 1697–1705
13. Van Eck, M., Zimmermann, R., Groot, P. H., Zechner, R., and Van Berkel, T. J. (2000) Role of macrophage-derived lipoprotein lipase in lipoprotein metabolism and atherosclerosis. *Arterioscler Thromb. Vasc. Biol.* **20**, E53–E62
14. Takahashi, M., Yagyu, H., Tazoe, F., Nagashima, S., Ohshiro, T., Okada, K., *et al.* (2013) Macrophage lipoprotein lipase modulates the development of atherosclerosis but not adiposity. *J. Lipid Res.* **54**, 1124–1134
15. Wilson, K., Fry, G. L., Chappell, D. A., Sigmund, C. D., and Medh, J. D. (2001) Macrophage-specific expression of human lipoprotein lipase accelerates atherosclerosis in transgenic apolipoprotein E knockout mice but not in C57BL/6 mice. *Arterioscler Thromb. Vasc. Biol.* **21**, 1809–1815
16. Aryal, B., Rotllan, N., Araldi, E., Ramirez, C. M., He, S., Chousterman, B. G., *et al.* (2016) ANGPTL4 deficiency in haematopoietic cells promotes monocyte expansion and atherosclerosis progression. *Nat. Commun.* **7**, 12313
17. Zilversmit, D. B. (1979) Atherogenesis: A postprandial phenomenon. *Circulation* **60**, 473–485
18. Yla-Herttuala, S., Lipton, B. A., Rosenfeld, M. E., Goldberg, I. J., Steinberg, D., and Witztum, J. L. (1991) Macrophages and smooth muscle cells

express lipoprotein lipase in human and rabbit atherosclerotic lesions. *Proc. Natl. Acad. Sci. U S A.* **88**, 10143–10147
19. O'Brien, K. D., Gordon, D., Deeb, S., Ferguson, M., and Chait, A. (1992) Lipoprotein lipase is synthesized by macrophage-derived foam cells in human coronary atherosclerotic plaques. *J. Clin. Invest.* **89**, 1544–1550
20. Weisberg, S. P., McCann, D., Desai, M., Rosenbaum, M., Leibel, R. L., and Ferrante, A. W., Jr. (2003) Obesity is associated with macrophage accumulation in adipose tissue. *J. Clin. Invest.* **112**, 1796–1808
21. Suganami, T., Tanaka, M., and Ogawa, Y. (2012) Adipose tissue inflammation and ectopic lipid accumulation. *Endocr. J.* **59**, 849–857
22. Garcia-Arcos, I., Hiyama, Y., Drosatos, K., Bharadwaj, K. G., Hu, Y., Son, N. H., *et al.* (2013) Adipose-specific lipoprotein lipase deficiency more profoundly affects brown than white fat biology. *J. Biol. Chem.* **288**, 14046–14058
23. Gao, J., Katagiri, H., Ishigaki, Y., Yamada, T., Ogihara, T., Imai, J., *et al.* (2007) Involvement of apolipoprotein E in excess fat accumulation and insulin resistance. *Diabetes* **56**, 24–33
24. Pakshir, P., Noskovicova, N., Lodyga, M., Son, D. O., Schuster, R., Goodwin, A., *et al.* (2020) The myofibroblast at a glance. *J. Cell Sci* **133**. jcs227900
25. Guzman-Ruiz, R., Tercero-Alcazar, C., Lopez-Alcala, J., Sanchez-Ceinos, J., Malagon, M. M., and Gordon, A. (2021) The potential role of the adipokine HMGB1 in obesity and insulin resistance. Novel effects on adipose tissue biology. *Mol. Cell Endocrinol* **536**, 111417
26. Mosser, D. M., and Edwards, J. P. (2008) Exploring the full spectrum of macrophage activation. *Nat. Rev. Immunol.* **8**, 958–969
27. Wentworth, J. M., Naselli, G., Brown, W. A., Doyle, L., Phipson, B., Smyth, G. K., *et al.* (2010) Pro-inflammatory CD11c+CD206+ adipose tissue macrophages are associated with insulin resistance in human obesity. *Diabetes* **59**, 1648–1656
28. Shaul, M. E., Bennett, G., Strissel, K. J., Greenberg, A. S., and Obin, M. S. (2010) Dynamic, M2-like remodeling phenotypes of CD11c+ adipose tissue macrophages during high-fat diet–induced obesity in mice. *Diabetes* **59**, 1171–1181
29. Khan, T., Muise, E. S., Iyengar, P., Wang, Z. V., Chandalia, M., Abate, N., *et al.* (2009) Metabolic dysregulation and adipose tissue fibrosis: Role of collagen VI. *Mol. Cell Biol* **29**, 1575–1591
30. Pasarica, M., Gowronska-Kozak, B., Burk, D., Remedios, I., Hymel, D., Gimble, J., *et al.* (2009) Adipose tissue collagen VI in obesity. *J. Clin. Endocrinol. Metab.* **94**, 5155–5162
31. Spencer, M., Yao-Borengasser, A., Unal, R., Rasouli, N., Gurley, C. M., Zhu, B., *et al.* (2010) Adipose tissue macrophages in insulin-resistant subjects are associated with collagen VI and fibrosis and demonstrate alternative activation. *Am. J. Physiol. Endocrinol. Metab.* **299**, E1016–E1027
32. McCulloch, L. J., Rawling, T. J., Sjoholm, K., Franck, N., Dankel, S. N., Price, E. J., *et al.* (2015) COL6A3 is regulated by leptin in human adipose tissue and reduced in obesity. *Endocrinology* **156**, 134–146
33. Jager, M., Lee, M. J., Li, C., Farmer, S. R., Fried, S. K., and Layne, M. D. (2018) Aortic carboxypeptidase-like protein enhances adipose tissue stromal progenitor differentiation into myofibroblasts and is upregulated in fibrotic white adipose tissue. *PLoS One* **13**, e0197777
34. Marcelin, G., Ferreira, A., Liu, Y., Atlan, M., Aron-Wisnewsky, J., Pelloux, V., *et al.* (2017) A PDGFRalpha-mediated switch toward CD9(high) adipocyte progenitors controls obesity-induced adipose tissue fibrosis. *Cell Metab* **25**, 673–685
35. Zhou, Y., Yu, X., Chen, H., Sjoberg, S., Roux, J., Zhang, L., *et al.* (2015) Leptin deficiency shifts mast cells toward anti-inflammatory actions and protects mice from obesity and diabetes by polarizing M2 macrophages. *Cell Metab* **22**, 1045–1058
36. Stienstra, R., Dijk, W., van Beek, L., Jansen, H., Heemskerk, M., Houtkooper, R. H., *et al.* (2014) Mannose-binding lectin is required for the effective clearance of apoptotic cells by adipose tissue macrophages during obesity. *Diabetes* **63**, 4143–4153
37. Beisiegel, U., Weber, W., and Bengtsson-Olivecrona, G. (1991) Lipoprotein lipase enhances the binding of chylomicrons to low density lipoprotein receptor-related protein. *Proc. Natl. Acad. Sci. U S A.* **88**, 8342–8346
38. Ge, X., Arriazu, E., Magdaleno, F., Antoine, D. J., Dela Cruz, R., Theise, N., *et al.* (2018) High mobility group box-1 drives fibrosis progression signaling via the receptor for advanced glycation end products in mice. *Hepatology* **68**, 2380–2404
39. Chang, H. R., Josefs, T., Scerbo, D., Gumaste, N., Hu, Y., Huggins, L. A., *et al.* (2019) Role of LpL (lipoprotein lipase) in macrophage polarization in vitro and in vivo. *Arterioscler Thromb. Vasc. Biol.* **39**, 1967–1985
40. Saraswathi, V., and Hasty, A. H. (2006) The role of lipolysis in mediating the proinflammatory effects of very low density lipoproteins in mouse peritoneal macrophages. *J. Lipid Res.* **47**, 1406–1415
41. Biswas, S. K., and Mantovani, A. (2012) Orchestration of metabolism by macrophages. *Cell Metab* **15**, 432–437
42. Wu, H., and Ballantyne, C. M. (2017) Skeletal muscle inflammation and insulin resistance in obesity. *J. Clin. Invest.* **127**, 43–54
43. Sekiya, M., Osuga, J., Okazaki, H., Yahagi, N., Harada, K., Shen, W. J., *et al.* (2004) Absence of hormone-sensitive lipase inhibits obesity and adipogenesis in Lep ob/ob mice. *J. Biol. Chem.* **279**, 15084–15090
44. Blank, T., and Prinz, M. (2016) CatacLysMic specificity when targeting myeloid cells? *Eur. J. Immunol.* **46**, 1340–1342
45. Wang, H., Astarita, G., Taussig, M. D., Bharadwaj, K. G., DiPatrizio, N. V., Nave, K. A., *et al.* (2011) Deficiency of lipoprotein lipase in neurons modifies the regulation of energy balance and leads to obesity. *Cell Metab.* **13**, 105–113
46. De Luca, S. N., Miller, A. A., Sominsky, L., and Spencer, S. J. (2020) Microglial regulation of satiety and cognition. *J. Neuroendocrinol* **32**, e12838
47. Augustus, A., Yagyu, H., Haemmerle, G., Bensadoun, A., Vikramadithyan, R. K., Park, S. Y., *et al.* (2004) Cardiac-specific knock-out of lipoprotein lipase alters plasma lipoprotein triglyceride metabolism and cardiac gene expression. *J. Biol. Chem.* **279**, 25050–25057
48. Kimura, H., Karasawa, T., Usui, F., Kawashima, A., Endo, Y., Kobayashi, M., *et al.* (2016) Caspase-1 deficiency promotes high-fat diet-induced adipose tissue inflammation and the development of obesity. *Am. J. Physiol. Endocrinol. Metab.* **311**, E881–E890
49. Takei, S., Nagashima, S., Takei, A., Yamamuro, D., Wakabayashi, T., Murakami, A., *et al.* (2020) Beta-cell-specific deletion of HMG-CoA (3-hydroxy-3-methylglutaryl-coenzyme A) reductase causes overt diabetes due to reduction of beta-cell mass and impaired insulin secretion. *Diabetes* **69**, 2352–2363
50. Nagashima, S., Yagyu, H., Tozawa, R., Tazoe, F., Takahashi, M., Kitamine, T., *et al.* (2015) Plasma cholesterol-lowering and transient liver dysfunction in mice lacking squalene synthase in the liver. *J. Lipid Res.* **56**, 998–1005
51. Takei, A., Nagashima, S., Takei, S., Yamamuro, D., Murakami, A., Wakabayashi, T., *et al.* (2020) Myeloid HMG-CoA reductase determines adipose tissue inflammation, insulin resistance, and hepatic steatosis in diet-induced obese mice. *Diabetes* **69**, 158–164